



CSUG/SPE 138168

The Effect of Heterogeneity on the Character of Density-Driven Natural Convection of CO₂ Overlying a Brine Layer

R. Farajzadeh, SPE and Shell International Exploration and Production, P. Ranganathan, SPE, P.L.J. Zitha, SPE, and J. Bruining, SPE, Delft University of Technology, The Netherlands

Copyright 2010, Society of Petroleum Engineers

This paper was prepared for presentation at the Canadian Unconventional Resources & International Petroleum Conference held in Calgary, Alberta, Canada, 19–21 October 2010.

This paper was selected for presentation by a CSUG/SPE program committee following review of information contained in an abstract submitted by the author(s). Contents of the paper have not been reviewed by the Society of Petroleum Engineers and are subject to correction by the author(s). The material does not necessarily reflect any position of the Society of Petroleum Engineers, its officers, or members. Electronic reproduction, distribution, or storage of any part of this paper without the written consent of the Society of Petroleum Engineers is prohibited. Permission to reproduce in print is restricted to an abstract of not more than 300 words; illustrations may not be copied. The abstract must contain conspicuous acknowledgment of SPE copyright.

Abstract

The efficiency of mixing in density-driven natural-convection is largely governed by the aquifer permeability, which is heterogeneous in practice. The character (fingering, stable mixing or channeling) of flow-driven mixing processes depends primarily on the permeability heterogeneity character of the aquifer, i.e., on its degree of permeability variance (Dykstra-Parsons coefficient) and the correlation length. Here we follow the ideas of Waggoner et al. (1992) to identify different flow regimes of a density-driven natural convection flow by numerical simulation. Heterogeneous fields are generated with the spectral method of Shinozuka and Jan (1972), because the method allows the use of power-law variograms. We observe from our simulations that the rate of mass transfer of CO₂ into water is higher for heterogeneous media.

1. Introduction

Efficient storage of carbon dioxide (CO₂) in aquifers requires dissolution in the aqueous phase. Indeed the volume available for gaseous CO₂ is less than for dissolved CO₂. The inverse partial molar volume (virtual density) of dissolved CO₂ is around 1300 kg/m³ (Gmelin, 1973) leading to more efficient storage than CO₂ remaining in the supercritical state (< 600 kg/m³) at relevant storage temperatures. Moreover, dissolution of CO₂ in water decreases the risk of CO₂ leakage. The mass transfer between CO₂ and underlying brine in aquifers causes a local density increase (Gmelin, 1973), which induces convection currents accelerating the rate of CO₂ dissolution (Yang and Gu, 2006; Farajzadeh et al, 2006, 2009). This system is gravitationally unstable and leads to unstable mixing enhancement in the aquifer (Riaz et al, 2006; Meulenbroek et al, 2010; Hassanzadeh et al, 2007; Farajzadeh et al, 2007).

The effect of natural convection increases with increasing Rayleigh number, which, for a constant-pressure CO₂-injection scheme, mainly depends on the permeability. This means that the efficiency of the mixing (caused by natural convection) is largely governed by the aquifer permeability (Green et al, 2009; Farajzadeh et al, 2007a), which is subject to spatial and directional variations in practice. Previous studies on this subject are mostly concerned with homogeneous porous media and despite attention of a few papers (e.g. Farajzadeh et al., 2008; Green et al, 2009; Nield and Simmons, 2007; Ranganathan et al, 2010) the effect of heterogeneity on the CO₂ mass transfer in aquifers is not fully understood.

Fingering is the dominant flow pattern in density driven natural convection flows in homogeneous media (Riaz et al, 2006, Farajzadeh et al, 2007a). However, CO₂ transport in heterogeneous media will be different than in homogeneous media because in the former case the permeability variations results in time-dependent velocity fluctuations, which in turn influence the mixing process. Waggoner et al. (1992) investigated flow regimes for miscible displacement through permeable media under vertical-equilibrium (VE) conditions. Depending on the degree of heterogeneity (represented by the Dykstra-Parsons coefficient, V_{DP}) and continuity of the system (correlation length λ_R), they distinguished flow regimes that are dominated by

fingering, dispersion, and channeling. The mixing zone displays different characteristics in these respective regimes. Mixing grows with the square root of time if dispersion dominates, whereas the growth is linear for displacements dominated by channeling and fingering. The principal difference between fingering and channeling is that a fingering displacement becomes dispersive when mobility ratio is less than one whereas a channeling displacement keeps the same character, albeit to a lesser degree. The work of Waggoner et al. is extended by Sorbie et al (1994) for more general cases and by Chang et al (1994), who include density variations. Based on these studies viscous fingering is dominant pattern in laboratory scale (or in quasi-homogeneous fields), but does not occur in the field where V_{DP} typically varies between 0.6 and 0.8 (in some exceptional cases V_{DP} can have values as large 0.9).

The aim of this paper is to investigate the effect of heterogeneity on the character of natural-convection flow of CO_2 in aquifers and on the dissolution rate of CO_2 in brine. The permeability fields were generated using the Dykstra-Parson coefficient, V_{DP} (measure of extent of heterogeneity) and spatial correlation length, λ_R (indicator of permeability-field correlation) as characterizing parameters. We follow the approach proposed by Waggoner et al. (1992) to characterize flow regimes (fingering, dispersive, and channeling) corresponding to density-driven natural-convection flow of CO_2 . The structure of the paper is as follows: First we describe the formulation of the physical model and introduce the ensuing equations. Then we briefly explain the method used to generate the permeability fields. Next we demonstrate the simulation results, and discuss their implications. We end the paper with some concluding remarks.

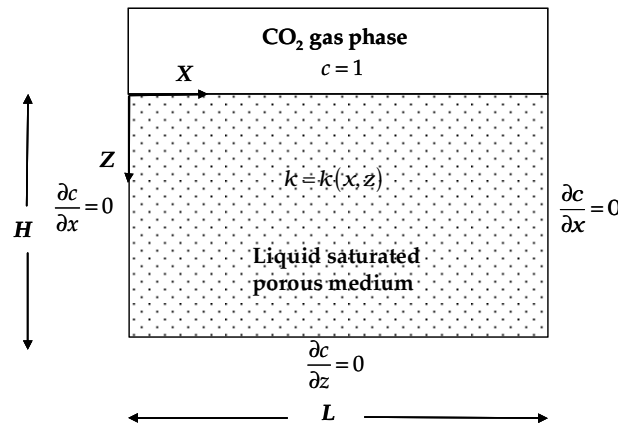


Figure 1: Schematic of the system and coordinates.

2. Physical Model

2.1. Formulation

We consider a fluid saturated porous medium with a height H and length L . The constant porosity of the porous medium is ϕ and its permeability varies spatially, i.e., $k = k(x, z)$. Initially the fluid is at rest and there is no CO_2 dissolved in the fluid. We assume no flow boundary at the sides and the bottom of the porous medium. CO_2 is continuously supplied from the top, i.e., the CO_2 concentration at the top is kept constant. We assume that the CO_2 -liquid interface is relatively sharp and fixed. We disregard the presence of a capillary transition zone between the gas and the liquid phase. Hence we only model the liquid phase and the presence of the gas phase at the top is represented by a boundary condition for the liquid phase. The motion of fluid is described by Darcy's law driven by a density gradient. Darcy's law is combined with the mass conservation laws for the two components (CO_2 and either water or oil) to describe the diffusion and natural-convection processes in the porous medium. We only expect a laminar regime since the Rayleigh number is low. We use the Boussinesq approximation which considers density variations only when they contribute directly to the fluid motion.

2.2. Governing equations

For the 2D porous medium depicted in Figure 1, the governing equations can be written as

(a) Continuity Equation

$$\phi \frac{\partial \rho}{\partial t} + \frac{\partial (\rho U_x)}{\partial X} + \frac{\partial (\rho U_z)}{\partial Z} = 0, \quad (1)$$

(b) Darcy's law

$$U_x = -\frac{k_m f(X, Z)}{\mu} \frac{\partial p}{\partial X}, \quad (2)$$

$$U_z = -\frac{k_m f(X, Z)}{\mu} \left(\frac{\partial p}{\partial Z} + \rho g \right) \quad , \quad (3)$$

(c) Concentration

$$\frac{\partial c'}{\partial t} + U_x \frac{\partial c'}{\partial X} + U_z \frac{\partial c'}{\partial Z} = \phi D \left(\frac{\partial^2 c'}{\partial X^2} + \frac{\partial^2 c'}{\partial Z^2} \right) \quad . \quad (4)$$

CO₂ dissolution at the top increases the fluid density. We assume that the liquid density changes linearly with the increasing CO₂ concentration, i.e.,

$$\rho = \rho_0 (1 + \beta_c (c' - c'_0)) \quad , \quad (5)$$

from which we obtain

$$\frac{\partial \rho}{\partial X} = \rho_0 \beta_c \frac{\partial c'}{\partial X} \quad . \quad (6)$$

In Eqs. (1)-(4) we have four unknowns (U_x , U_z , p , and c'). It is possible to eliminate the pressure by differentiating Eq. (2) with respect to Z and Eq. (3) with respect to X and subtract the result. This leads to

$$\frac{\partial U_z}{\partial X} - \frac{\partial U_x}{\partial Z} = \frac{k(X, Z) g \rho_0 \beta_c}{\mu} \frac{\partial c'}{\partial X} \quad . \quad (7)$$

Therefore, the equations to be solved are Eqs. (1), (4) and (7) to obtain U_x , U_z and c' .

2.3. Dimensionless form of the equations

We take H as characteristic length and define the following dimensionless variables

$$x = \frac{X}{H}, \quad z = \frac{Z}{H}, \quad u_x = \frac{H}{\phi D} U_x, \quad u_z = \frac{H}{\phi D} U_z, \quad \tau = \frac{D}{H^2} t, \quad c = \frac{c' - c'_i}{c'_0 - c'_i}$$

$$u_x = -\frac{\partial \psi}{\partial z}, \quad u_z = \frac{\partial \psi}{\partial x}, \quad \text{Ra} = \frac{k_m \rho_0 \beta_c g H \Delta c'}{\phi D \mu} = \frac{\Delta \rho g k_m H}{\phi D \mu} \quad (8)$$

Thus, after applying the Boussinesq approximation the dimensionless form of the equations can be written as

$$\frac{\partial}{\partial x} \left(\frac{1}{k(x, z)} \frac{\partial \psi}{\partial x} \right) + \frac{\partial}{\partial z} \left(\frac{1}{k(x, z)} \frac{\partial \psi}{\partial z} \right) = \text{Ra} \frac{\partial c}{\partial x} \quad , \quad (9)$$

and,

$$\frac{\partial c}{\partial \tau} - \frac{\partial \psi}{\partial z} \frac{\partial c}{\partial x} + \frac{\partial \psi}{\partial x} \frac{\partial c}{\partial z} = \frac{\partial^2 c}{\partial x^2} + \frac{\partial^2 c}{\partial z^2} \quad . \quad (10)$$

2.4. Boundary and initial conditions

The initial condition of the problem is

$$\psi = 0, \quad c = 0 \quad \text{at} \quad \tau = 0 \quad , \quad (11)$$

The boundary conditions of the problem are

$$\psi = 0, \quad \frac{\partial c}{\partial z} = 0 \quad \text{at} \quad x = 0, \quad \psi = 0, \quad c = 1 \quad \text{at} \quad z = 0, \quad \psi = 0, \quad \frac{\partial c}{\partial x} = 0 \quad \text{at} \quad z = 1, \quad \psi = 0, \quad \frac{\partial c}{\partial x} = 0 \quad \text{at} \quad x = A. \quad (12)$$

2.5. Solution procedure

A modified version of the numerical method explained by Guçeri and Farouk (1985), i.e., the finite volume approach, was applied to solve the system of equations (9) and (10). A fully implicit method was used to obtain the transient values in equation (10). For each time step, we first compute the stream function from equation (9) and then we obtain the concentration profile by solving equation (10). The calculation procedure for each time step was repeated until the following criteria were satisfied

$$\left| \frac{C_{i,j}^{\tau+\Delta\tau} - C_{i,j}^{\tau}}{C_{i,j}^{\tau+\Delta\tau}} \right|_{\max} \leq \varepsilon \quad \text{and} \quad \left| \frac{\psi_{i,j}^{\tau+\Delta\tau} - \psi_{i,j}^{\tau}}{\psi_{i,j}^{\tau+\Delta\tau}} \right|_{\max} \leq \varepsilon, \quad (13)$$

where ε was set to 10^{-5} in the numerical computations reported in this paper and the time step was chosen to be 10^{-5} ($V_{DP} < 0.8$) and 10^{-6} ($V_{DP} = 0.8$) to obtain accurate results.

To observe the non-linear behavior, i.e., the fingering behavior it was necessary to disturb the interface. Therefore in the numerical simulations, we start with a wavy perturbation on the top interface, i.e.,

$$c(x, z = 0, t = 0) = 1 + A_0 \sin(2\pi x / \lambda), \quad (14)$$

where $A_0 = 0.01$ and $\lambda = 1/12$. In reality fluctuations are caused by thermodynamic fluctuations (see Landau and Lifshitz, 1969; Gunn and Krantz, 1980) and pore-level perturbations. We ignore instabilities on the pore level (see, however, e.g. Yortsos et al, 1997; Parlar and Yortsos, 1987).

2.6 Interpretation

2.6.1. Effective dispersion coefficient

It is our aim to derive the character of the of the displacement process, i.e., whether it is mainly diffusive or convective. To interpret the result we adapt the method explained in detail in Gelhar (1993). First we average the concentration profile in the x -direction and divide by the concentration at the gas-liquid boundary to obtain $\partial\hat{c}(z, t)$. This concentration can be considered as a complementary cumulative distribution function and its derivative towards z as a probability density function. For convenience we add the symmetric part to the probability density function $p(z, t)$ such that

$$p(z, t) = -\frac{1}{2} \left(\frac{\partial\hat{c}(|z|, t)}{\partial z} \right) \quad (15)$$

The variance σ_c^2 of the concentration profile is given by,

$$\sigma_c^2 = 2 \int_0^\infty z^2 p(z, t) dz = 2 \int_0^\infty z \hat{c}(|z|, t) dz \quad (16)$$

where we used integration by parts. If the process were purely diffusive we would obtain that $\hat{c}(z, t) = \text{erfc}(z / 2\sqrt{Dt})$, where D is the diffusion coefficient. In this case $\sigma_c^2 = 2Dt$ and hence we will interpret $D(t) = 1/2 d\sigma_c^2 / dt$ as a diffusion coefficient. When the diffusion coefficient is independent of time the process is considered diffusive; if it is more proportional to time it is considered convective. If, in the latter case, the concentration profile develops along high permeability paths we will call it channeling, if it develops arbitrarily we call it fingering.

2.6.2. Other measures of heterogeneity

Coefficient of variation, C_V : The coefficient of variation is a measure of sample variation or dispersion and expresses the standard deviation, σ , as a fraction of sample mean, \bar{k} (Jensen et al, 1997, pp 128). It is defined as: $C_V = \sigma / \bar{k}$. Samples with $C_V < 0.5$ are considered homogeneous and with $C_V > 1$ are assumed very heterogeneous (Jensen et al., 1997, pp 130).

Koval factor, H_K : The Koval heterogeneity factor (Koval, 1963) is typically used to account for unstable behavior of miscible displacement in heterogeneous porous media. The relation between V_{DP} and H_K is:

$$\log_{10}(H_K) = V_{DP} / (1 - V_{DP})^{0.2}, \quad (17)$$

Heterogeneity index, I_H : Gelhar-Axness coefficient or heterogeneity index (Gelhar and Axness, 1983) combines the degree of heterogeneity with the correlation length as

$$I_H = \sigma_{\ln k}^2 \lambda_r, \quad (18)$$

where $\sigma_{\ln k}^2$ is the variance of log permeability fields and λ_r is the dimensionless correlation ($\lambda_r = \lambda / L$, where L is the system length).

Our aim is to find out whether there is a relation between the mass of dissolved CO_2 in water and the heterogeneity of the porous medium represented by one of the measures of heterogeneity. .

3. Generation of stochastic random fields

Random field generators are widely used as a tool to model heterogeneities in porous media (Lasseter et al, 1986) for applications in hydrocarbon recovery and groundwater flow. The generated field can be used as model (permeability) fields for research work (Waggoner et al., 1992). Prediction methods (King et al., 1993) for many realizations of such fields can quantify

the uncertainty of expected product recoveries.

A number of methods have been conventionally employed to generate random fields (Journel and Huijbregts, 1978; Deutsch and Journel, 1992, Bruining et al., 1997). First, we note that these conventional methods generate correlated random fields from a sum of terms and hence generate multi-Gaussian fields. Most earth-science phenomena are not multivariate Gaussian but can be transformed such that the resulting variable is approximately Gaussian for example the logarithm of the permeability (Jensen and Lake, 2000). This paper uses the Spectral (Fourier) methods (Rice, 1954; Shinozuka and Jan, 1972) to generate fields with exponential variograms (Bruining et al., 1997), which only involves correlation over a single length scale. We leave an analysis using a permeability field that involves many length scales (Bruining et al., 1997; Borges et al., 2009); fractal fields (Ebrahimi and Sahimi, 2006); wavelets (Elfeki et al., 2002; Dekking et al., 2001); Markov processes and non-Gaussian methods using Copula-based methods (Bárdossy, 2006) for future work.

We use the following equation of a random field value for a two-dimensional field:

$$f(x_1, x_2) = \sqrt{2} \sum_{k=-N/2}^{N/2-1} \sum_{l=-N/2}^{N/2-1} (S_2(\omega_{kl}) w(\omega_{1k}, \omega_{2l}))^{1/2} \cos(\omega_{1k} x_1 + \omega_{2l} x_2 + \phi_{kl}) \quad (19)$$

The proof that Equation (19) gives a field with the correct expected statistical properties is reproduced in Bruining et al. (1997). In the equation, the indices 1 and 2 denote the x and z -direction. Application of Eq. (19) requires further information on the phase angle ω_{kl} , the spectral density function $S_2(\omega_{kl})$, the distribution of summation points and the weighting function $w(\omega_{1k}, \omega_{2l})$. To avoid the occurrence of spurious symmetry patterns we added a small random frequency $\delta\omega$ to ω_{1k}, ω_{2l} , i.e., $\delta\omega = 0.05\pi / ((N-1)b) U(0,1-1/2)$, where $U(0,1)$ denotes a uniformly distributed random variable with average zero and standard deviation one. The random phase angle ϕ_{kl} is distributed uniformly between 0 and 2π . In the spectral density function, denoted by $S_2(\omega_{kl})$, we use the abbreviation $\omega_{kl} = \sqrt{(\omega_{1k}^2 + \omega_{2l}^2)}$ and the subscript 2 to denote 2D. The spectral density function (Mantoglou and Wilson, 1982) corresponding to the exponential variogram $\gamma(h) = s^2(1 - \exp(-h/\lambda))$ reads:

$$S_2(\omega) = \frac{s^2}{2\pi} \frac{1/\lambda}{(\omega^2 + 1/\lambda^2)^{3/2}} \quad (20)$$

Equation (19) represents a Fourier transform. Consequently, we use frequencies $\omega_{1k}; \omega_{2l}$ in the range $[-\pi/b, \pi/b]$ where b is the distance between points. Also Nb is the system length and $\Delta\omega = 2\pi/(bN)$. We employ the full autocorrelation structure of the field only if the integral of the spectral density function over the thus-defined frequency space approaches σ^2 . In other words, it is only useful to generate a field with a certain autocorrelation structure if the points in space are distributed sufficiently densely such that they indeed contain the information on the complete spectral density function (Press et al., 1992 p. 500). Indeed, the preservation of the statistical properties depends only on having a sufficiently large number of points to get a reasonably distributed set of phase angles ϕ_{kl} at enough locations to accurately and completely sample the spectral density. As shown in Bruining et al. (1997), fast Fourier transform algorithms do not always (Monnig et al (2008)) give fields with the correct statistical properties.

The function $f(x_1, x_2)$ generated in Eq. (19) is normally distributed due to the central limit theorem and in its standard normal form. In many cases of practical interest the logarithm of the permeability is normally distributed (Jensen et al. (2000)). In this case the logarithm of the permeability can be expressed by $\ln k = \mu + s f(x_1, x_2)$, where μ is the geometric average of the permeability k and $s = -\ln(1 - V_{DP})$ is the standard deviation of $\ln k$. The Dykstra-Parson coefficient V_{DP} is a measure of heterogeneity and assumes values in the range (0.6, 0.8) and exceptionally up to (0.9) in cases of practical interest. It is therefore that the correlation structure of $\ln(k)$ is given by $\gamma_{nk}(h) = s^2(1 - \exp(-h/\lambda))$ if this structure is indeed exponential. It can be shown (Vanmarcke, 1983) that the variogram of k reads

$$\gamma_k(h) = \sigma^2 \frac{1 - e^{-\gamma_{nk}(h)}}{1 - e^{-s^2}}, \quad (15)$$

where $\sigma^2 = \exp(2\mu + s^2) (\exp(s^2) - 1)$ is the variance of k . The average value of $k = \exp(\mu + 1/2 s^2)$.

We have used Eq. (19) to generate 81×81 fields for $k = \exp(\mu + s f(x_1, x_2))$ using $N \times N = 201 \times 201$ frequency points. For each case with different values of V_{DP} and average permeability we generated 10 realizations of the fields by using different sequences of the random phase angles (ϕ_{kl}). As a rule of thumb we would need $(10 C_v)^2$ realizations (Jensen et al., 2000, pp 151), where $C_v = \sqrt{\exp(s^2) - 1}$ is the coefficient of variation (average / standard deviation) to obtain statistically meaningful results, but this is technically impossible, because it requires per case hundreds of simulations, which each take few hours. However, by taking ten realizations per case we will obtain some idea of the variations that can be expected for these highly heterogeneous permeability fields.

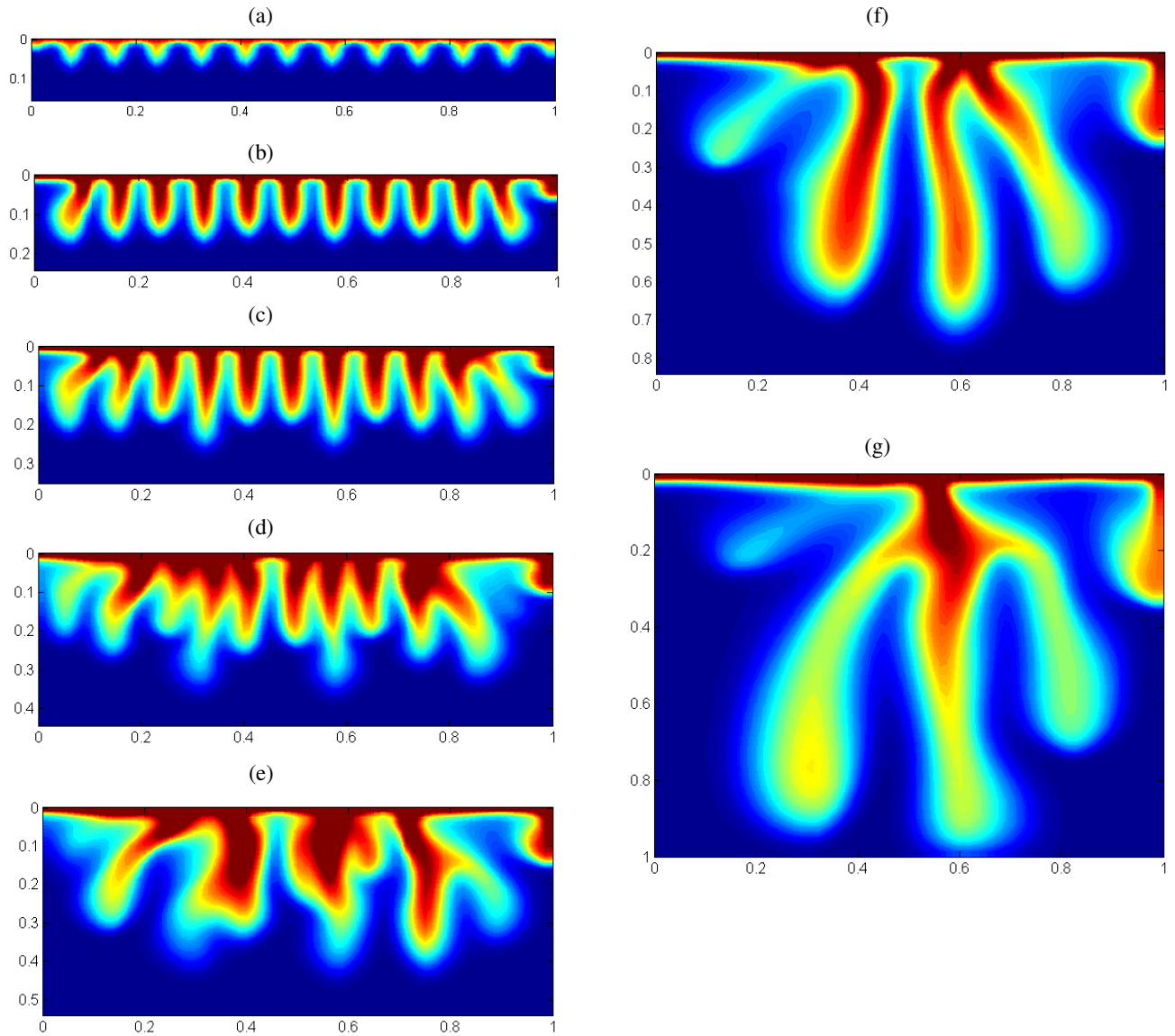


Figure 2: Concentration profiles of the base case (homogeneous medium and $Ra=5000$); at $\tau =$ (a) 0.0001, (b) 0.0003, (c) 0.0005, (d) 0.00075, (e) 0.001, (f) 0.0015 and (g) 0.002.

4. Results

4.1. Homogeneous case

Figure 2 shows the concentration profile of CO_2 for $Ra = 5000$ at different dimensionless times. The general features of the density-driven natural convection flow in a homogeneous porous medium are as follows (for details see Farajzadeh et al., 2007a):

- Initially, the behavior of the system is controlled by diffusion. The time at which convection starts to dominate the flow, τ_c , decreases with increasing Rayleigh number. It has been shown that $\tau_c \propto 1/Ra^2$ (Xu et al., 2006).
- At early times, e.g. Figure 2a and 2b, the number of fingers remain equal to the number put in the initial perturbation, i.e., 11.
- Some fingers grow faster than the others (Figure 2c). As time elapses number of fingers decreases (Figure 2d to 2g). The neighboring fingers coalesce by mutual interaction, and only few fingers survive to reach the bottom of the medium (Figure 2g).

- The concentration contours suggest that the late-stage behavior of the mass transfer process cannot be precisely predicted by the early-stage behavior of the system. There will be some tenacity of the initial behavior and the pattern observed in the figures persists for some time before the number of fingers starts to decrease and starts to reflect structural properties (see Figure 15 in Farajzadeh et al., 2007).
- The stream-function profile preserves a similar pattern as the concentration profile (Figure 3). This shows the importance of natural convection for the spreading of CO₂ in the cell. Moreover, it means that the dynamics of the non-linear behavior, i.e. fingering of CO₂ in the porous medium is governed by the flow field.
- The value of stream function decreases after reaching a maximum. This is in agreement with experimental observations indicating that convection effects diminish with time due to the increasingly more homogeneous concentration distribution as time progresses. The maximum Sherwood number or maximum value of the stream function is when CO₂ hits the bottom of the cell for the first time (Farajzadeh et al., 2007c & 2009).
- The concentration front moves faster for the larger Rayleigh numbers implying that natural convection affects the mass transfer significantly for larger Rayleigh numbers (or aquifers with higher permeability).

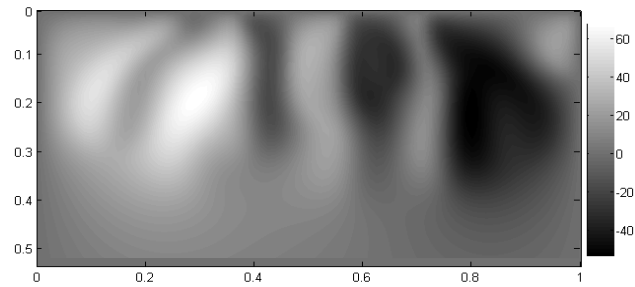


Figure 3: Stream-function profile for $Ra=5000$ at $\tau = 0.001$ corresponding to concentration profile in Figure 2e

4.2. Effect of heterogeneity

We follow the terminology proposed by Waggoner et al. (1992) to interpret density-driven natural convection in a heterogeneous medium characterized by an average Dykstra-Parsons coefficient and a correlation length. We did not consider viscosity variations in our simulations. CO₂ dissolution increases the brine viscosity (Bando et al., 2004) and therefore the flow will resemble favorable miscible displacement ($M < 1$) (Note that this reverse viscosity effect has impact on the initiation and growth of fingers especially when the effect of interface velocity (Haugen and Firoozabadi, 2009) is considered (Meulenbroek et al., 2010)). This means that for our situations we use $M = 1$. According to Waggoner et al (1992) fingers disappear when $M = 1$; however, our situation concerns gravity-induced fingering and fingering disappears when $M + G < 1$ (Dake, 1978).

Table 1: Labels of the permeability fields characterized by V_{DP} and λ_R .

Case ID	V_{DP}	λ_R	Case ID	V_{DP}	λ_R	Case ID	V_{DP}	λ_R	Case ID	V_{DP}	λ_R
P1P01	0.1	0.01	P3P01	0.3	0.01	P5P01	0.5	0.01	P8P01	0.8	0.01
P1P1	0.1	0.1	P3P1	0.3	0.1	P5P1	0.5	0.1	P8P1	0.8	0.1
P1P5	0.1	0.5	P3P5	0.3	0.5	P5P5	0.5	0.5	P8P5	0.8	0.5
P11	0.1	1	P31	0.3	1	P51	0.5	1	P81	0.8	1
P13	0.1	3	P33	0.3	3	P53	0.5	3	P83	0.8	3

We chose an average permeability that leads with other conditions to $Ra = 5000$. We generated 20 permeability fields represented by four levels of V_{DP} and λ_R . The V_{DP} values were 0.1, 0.3, 0.5, and 0.8. λ_R values were chosen to represent porous media from small to extremely large correlation; λ_R values were 0.001, 0.1, 0.5, 1, and 3. In all cases we chose $k_h = k_v$ and $L/H = 1$. To facilitate the discussion we have given a label to each case, as presented in Table 1 (P stands for point, the first number is V_{DP} and the second number is λ_R , e.g., Case P8P01 means the case with $V_{DP} = 0.8$ and $\lambda_R = 0.01$).

Table 2 summarizes examples of the output of our model for different realizations with $V_{DP} = 0.8$ and $\lambda_R = 1$. We notice that due to random nature of the stochastic model the output values are different for different realizations with the same input.

Table 3 provides the output of the program for $V_{DP} = 0.5$ and $V_{DP} = 0.8$ with different values for correlation length, λ_R . A variety of sample values related to the variance are calculated from output Rayleigh field of the two cases. We arbitrarily chose the seventh realization for this calculation. We observe that with increasing λ_R : (1) the estimated values of the heterogeneity index, the arithmetic and harmonic average increase, (2) the estimated values of V_{DP} , Koval factor and coefficient of variation decrease, and (3) the values of V_{DP} deviate further from the input value. Moreover, the sample variance is below the expected

variance, especially for large correlation length. If the correlation length becomes infinity the variance would be zero. The reduction of coefficient of variation implies that we need a smaller number of realizations to conclude about the character of flow.

Table 2: Output values of the stochastic model for input: $Ra = 5000$, $V_{DP} = 0.8$ ($\sigma_{\ln Ra} = 1.27$), and $\lambda_R = 1$.

Realization number	$\sigma_{\ln Ra}$	Output V_{DP}	Arithmetic average	Harmonic average	Heterogeneity Index (I_H)	Koval factor	Coefficient of variation
1	0.97	0.62	1417.7	562.8	5.70	0.90	1.23
2	1.05	0.65	5269.8	1795.7	6.36	1.23	1.39
3	0.87	0.58	4244.3	2020.6	4.89	0.56	1.05
4	0.83	0.56	12929.0	6507.7	4.63	0.48	0.99
5	0.69	0.50	3582.4	2213.5	3.77	0.23	0.77
6	0.97	0.62	3657.2	1511.5	5.67	0.88	1.19
7	1.08	0.66	98335.0	33054.1	6.58	1.35	1.40
8	0.80	0.55	21823.4	11628.1	4.42	0.41	0.94
9	0.76	0.53	539.2	303.5	4.17	0.33	0.88
10	0.87	0.58	5959.5	2884.4	4.93	0.58	1.03

Table 3: Output values of the stochastic model for input: $Ra = 5000$ for two V_{DP} values.

Input V_{DP}	Input λ_R	$\sigma_{\ln(Ra)}$	Output V_{DP}	Arithmetic average	Harmonic average	Heterogeneity Index (I_H)	Koval factor	Coefficient of variation
0.50	0.01	0.70	0.50	6422.2	3921.4	0.038	0.24	0.80
0.50	0.1	0.69	0.49	7888.2	4948.6	0.37	0.22	0.77
0.50	0.5	0.55	0.42	13413.9	9940.1	1.49	0.09	0.59
0.50	1	0.46	0.37	15445.6	12484.0	2.55	0.05	0.49
0.50	3	0.40	0.33	16132.2	13756.1	8.84	0.026	0.42
0.80	0.01	1.63	0.80	22347.3	1379.9	0.13	7.00	3.90
0.80	0.1	1.55	0.79	14244.3	1435.7	1.19	5.79	2.99
0.80	0.5	1.28	0.72	81241.1	17853.6	4.29	2.70	1.89
0.80	1	1.08	0.66	98335.0	33054.1	6.58	1.35	1.40
0.80	3	0.93	0.60	99797.8	43727.1	16.11	0.75	1.13

4.2.1 Fingering regime

At low V_{DP} independent of the correlation length we observe fingering behavior. By fingering we mean that the concentration plumes develop independently of the permeability structure. This aspect is illustrated in Figure 4. Figure 4a shows the Rayleigh (or permeability) field of one of the realizations of Case P13. Although the variance of the field is small ($\sigma_{\ln(Ra)}^2 = 0.0023$), we observe that at the north and northwest of the field some clusters of gridcells have about 10% higher permeability than the average value, whilst the gridcells in the east part have about 10% lower permeability. The plumes develop equally well in the west and the east parts of the field. Figures 4b to 4f depict the development of the plumes with time. The flow regime is similar to the homogeneous case explained in the previous section (Figure 2). Figure 5 shows the grey-level plot of the stream-function profile. The stream-function profile shows similar features as the concentration profile, i.e., the fingers are driven by the velocity profiles. The value of the stream function in this case is similar to the value in the homogenous case.

In Figures 11 we show the variance of the concentration profiles as function of dimensionless time (Eqs. (15) and (16)). For comparison, we present all results (with the exception of $V_{DP} = 0.1$) on this figure. In each plot we show results of multiple realizations of each case. For $V_{DP} = 0.1$ (not shown in the figure) and Case P33 (top left plot) the variance increases faster than linear for all realizations implying that the flow is not diffusive. In Figure 12 we present the cumulative mass dissolved as a function of time. The colored lines represent different realizations while the dashed line represents the dissolved mass of the homogeneous case on each plot. The mass transfer is slower than linear but faster than square-root of time showing the mixed diffusive-convective behavior in both homogeneous and heterogeneous media. When the correlation length is small the amount of dissolved CO_2 is larger than the homogeneous case for all of the realizations. When the correlation length becomes larger the mass of dissolved CO_2 in some realizations becomes lower than the homogenous case; however, the majority of the

realizations show higher mass transfer rates. Moreover, the transfer rates of different realizations deviate further from the mean value when the correlation length becomes larger (the distance between lines becomes larger).

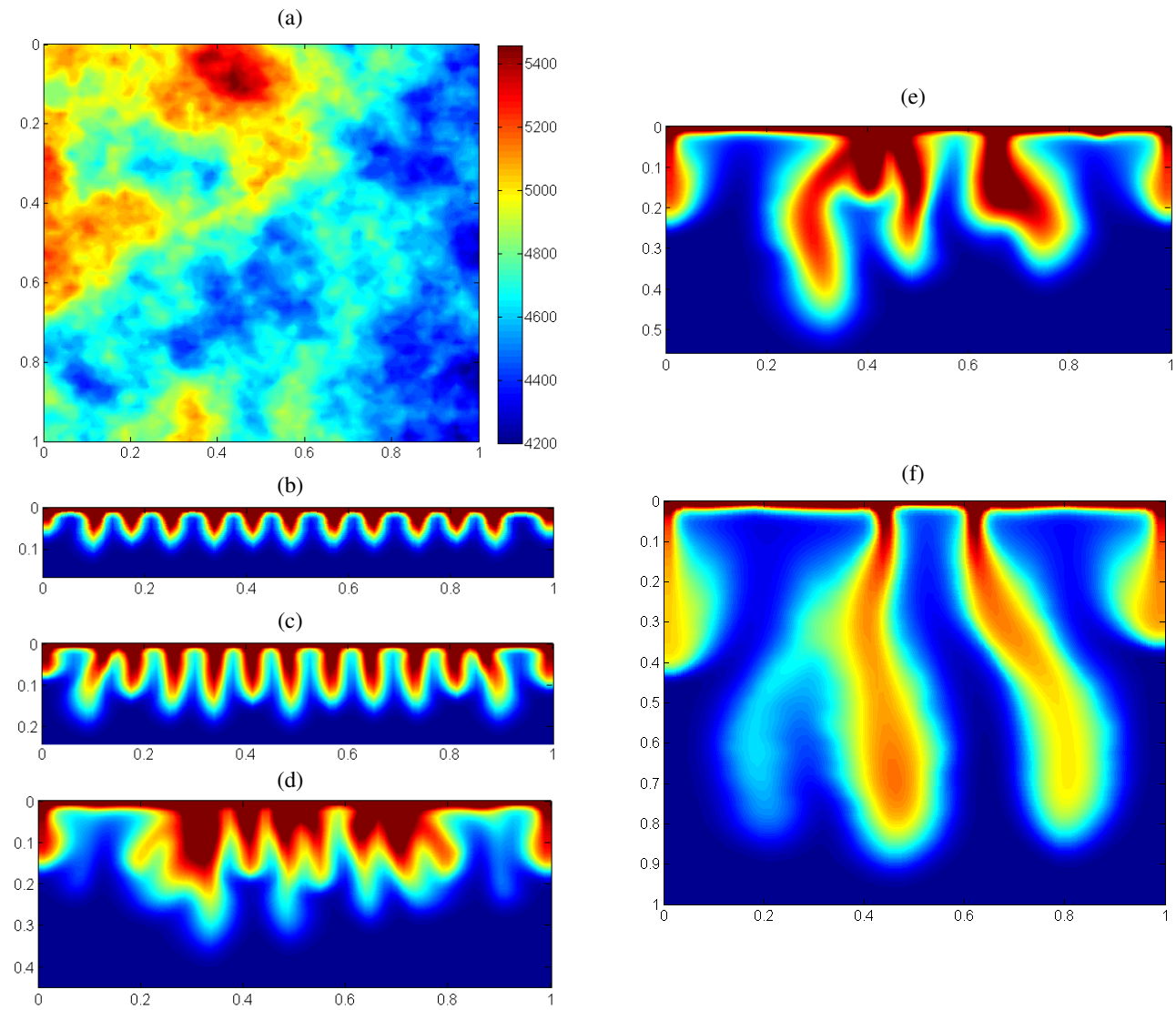


Figure 4: Rayleigh field and concentration profiles of $V_{Dp} = 0.1$ and $\lambda_R = 3$ (Case P13): at $\tau =$ (b) 0.0001, (c) 0.0003, (d) 0.00075, (e) 0.001, and (f) 0.002.

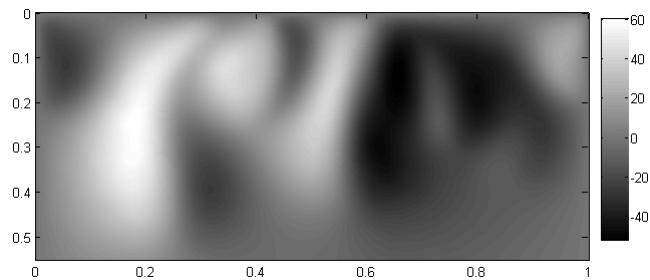


Figure 5: Stream-function profile for Case P13 at $\tau = 0.001$ corresponding to concentration profile in Figure 4e.

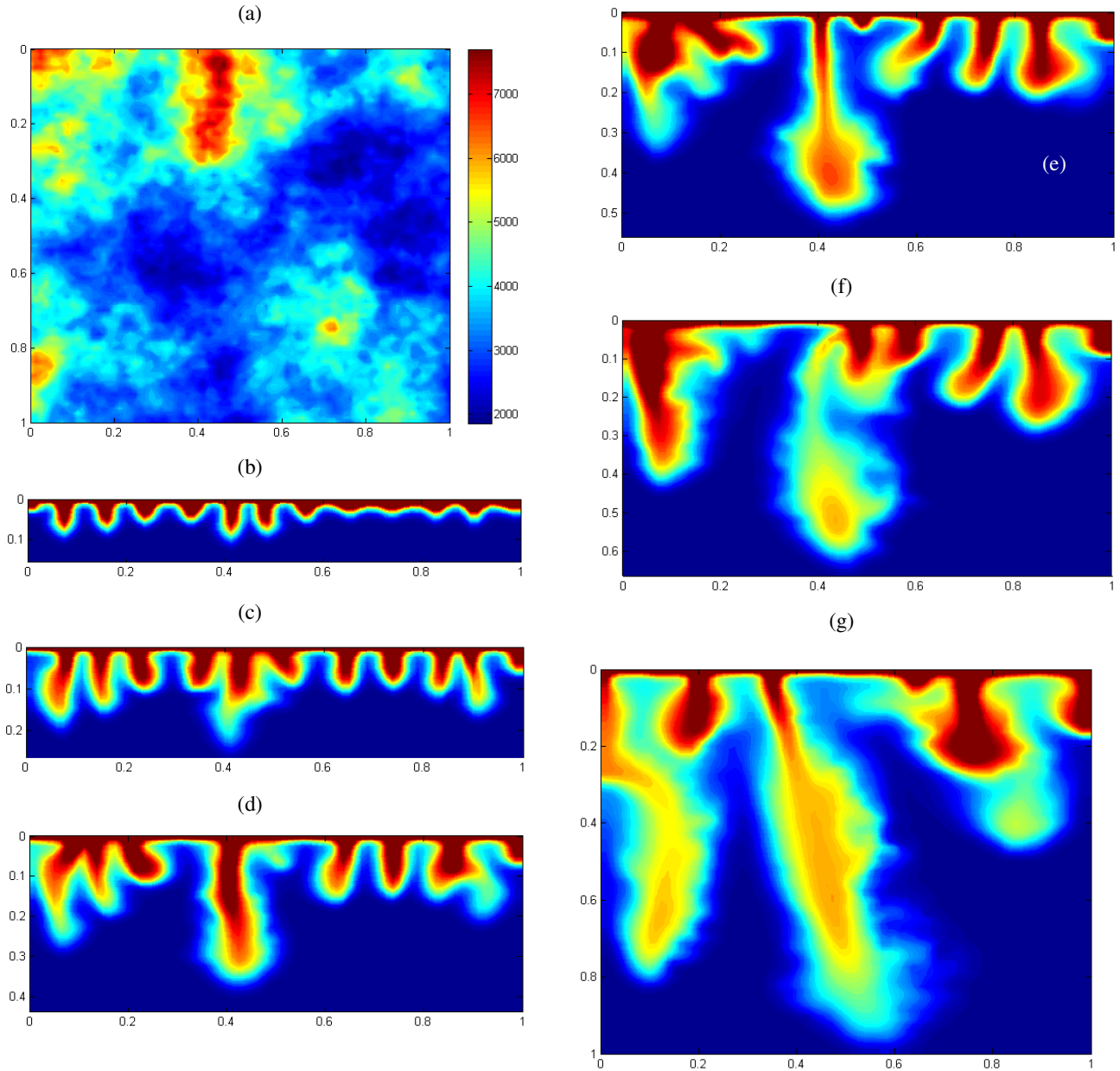


Figure 6: Rayleigh (permeability) field and concentration profiles of $V_{DP} = 0.5$ and $\lambda_R = 3$ (Case P53) at $\tau =$ (b) 0.0001, (c) 0.0003, (d) 0.0005, (e) 0.00075, (f) 0.001 and (g) 0.002.

4.2.2. Channeling regime

Channeling regime occurs for medium V_{DP} values (moderate heterogeneity) independent of the correlation length. Note that when the correlation length becomes large the estimated V_{DP} of the medium becomes smaller (Table 2 and Bruining et al., 1997). With channeling we mean that the plume develops along the high permeability streaks, i.e., the progress of CO_2 plumes are dominated by the permeability distribution pattern. An example of channeling is shown in Figure 6. Figure 6a shows the Rayleigh field of one of the realizations of Case P53. We observe high permeability streaks at the north and northwest parts of the field. Figure 6b to 6f show indeed that faster plume development occurs along the high permeability regions. Due to channeling water is bypassed and thus dissolution is not efficient. Because of the higher variance of the permeability field compared to the previous case ($\sigma_{\ln(Ra)}^2 = 0.01 > 0$), some of realizations show lower dissolution rate than the homogeneous case; however, in average the dissolution rate for heterogeneous media is higher than for the homogeneous case. Similar to the fingering regime, the growth of variance of concentration profile in corresponding plots in Figure 11 is faster than linear and slower than square root of time, implying mixed convective-dispersive flow. Figure 7 shows the stream-function profile of this

example. It illustrates that the fluid velocity is higher in high permeability region and lower in low permeability regions. The magnitude of the stream function is comparable to the fingering example.

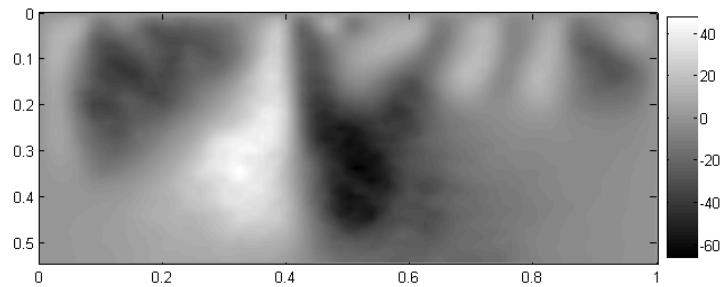


Figure 7: Stream-function profile for Case P53 at $\tau = 0.00075$ corresponding to concentration profile in Figure 6e.

4.2.3. Dispersive regime

For large heterogeneities when the correlation length is small, the concentration profile progresses proportional to the square root of the time. This regime is dispersive as bypassing of water in channels is not observed in the simulations and therefore the mixing is more efficient. Figure 8 shows the Rayleigh field of one of the cases in which we observe the dispersive behavior. The Rayleigh field has a very large variance ($\sigma_{\ln(Ra)}^2 = 2.25$) and contains grid cells with permeability values that are smaller than 100 and values larger than 10^6 . The concentration profile of this Rayleigh field is presented in Figures 9a through 9e. The mixing zone develops as a result of the physical dispersion plus the mixing caused by the heterogeneities of small λ_R . The time at which CO_2 reaches the bottom is larger than the fingering and channeling regimes and consequently the transfer rate of CO_2 is higher in the dispersive regime. As shown in Figure 11 the mixing zone in all realizations progresses proportional to the square root of the time. This implies that for fields with large variance and small correlation length, the mass transfer of CO_2 into water can be described with a dispersion model with large effective dispersion coefficient to account for the velocity induced by density-driven natural convection. Figure 10 shows the stream function profile of this case. As expected the stream function has very large values in high permeability grid cells (note the similarities between Figures 8 and 10).

Figure 13 shows the schematic diagram of the flow regime introduced by Waggoner et al. (1992). This plot is generated based on Figure 11, where we plot the variance of concentration profile as a function of time. For Case P83, from the simulations we observe that for all realizations the CO_2 plumes progress along the high permeable regions; however, as Figure 11 (top right plot) shows the plot of variance of concentration profile vs. time is linear implying the flow can be dispersive. Therefore, in Figure 13 for large heterogeneities the boundary between dispersive and channeling regimes has been shown by a dashed curve.

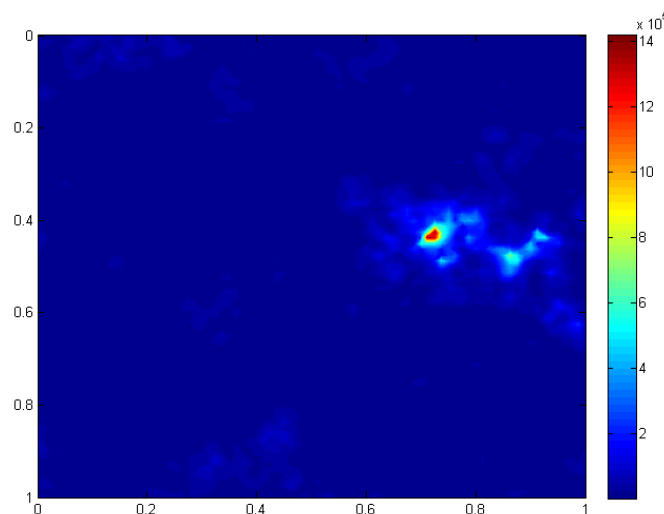


Figure 8: Rayleigh field of $V_{DP} = 0.8$ and $\lambda_R = 0.1$ (Case P8P1).

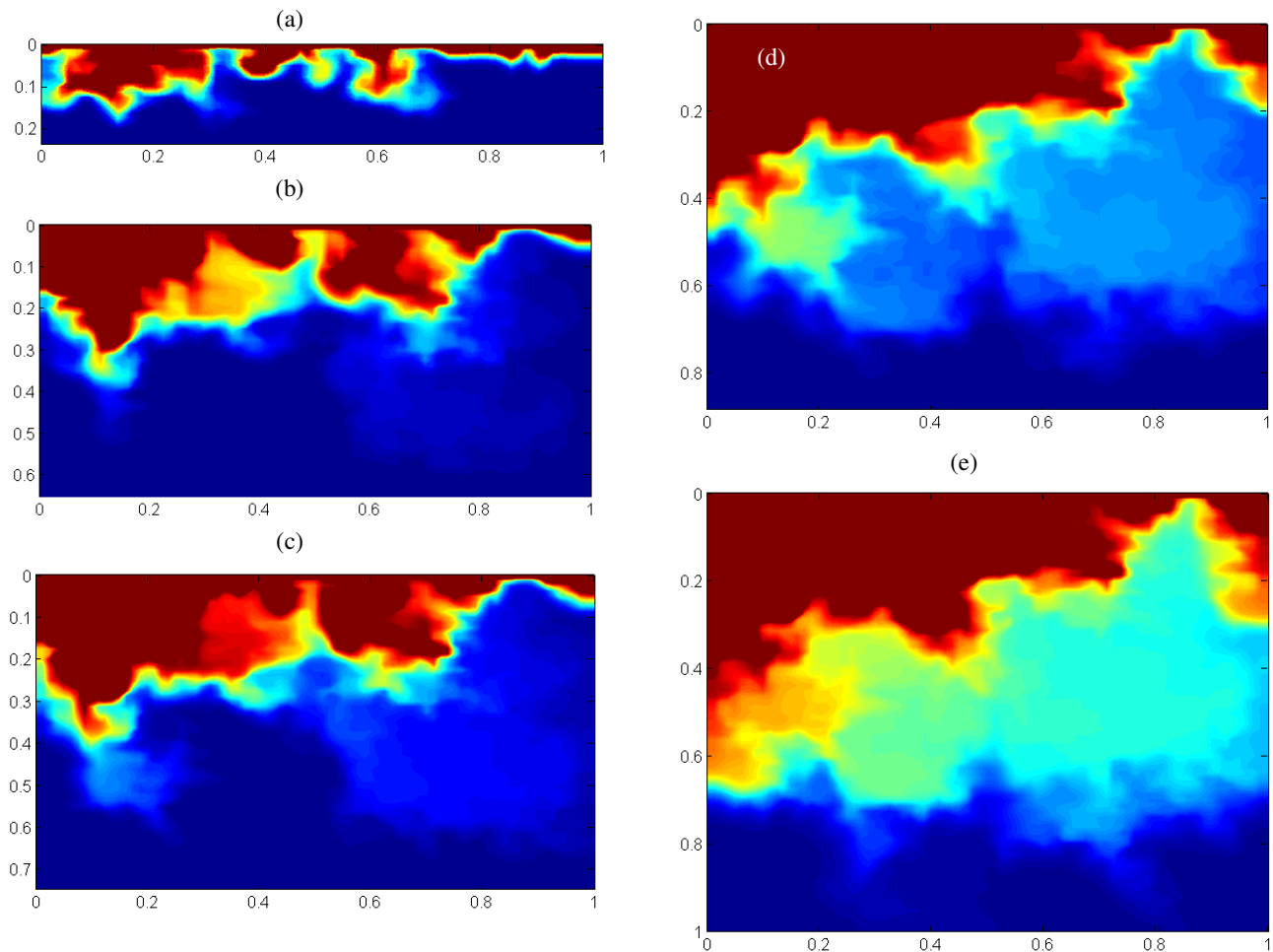


Figure 9: Concentration profiles of $V_{DP} = 0.8$ and $\lambda_R = 0.1$ (Case P8P1) at $\tau =$ (a) 0.0001, (b) 0.0005, (c) 0.00075, (d) 0.0015, and (e) 0.0025.

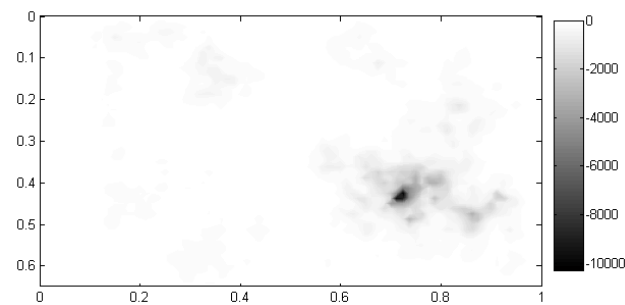


Figure 10: Stream-function profile for Case P8P1 at $\tau = 0.00075$ corresponding to concentration profile in Figure 8e.

4.2.4. Implications of the results

Aquifers (or reservoirs) are in general heterogeneous with V_{DP} values typically between 0.6 and 0.8 (and even higher). Our results show that gravity-induced fingering does not occur in realistic porous media, i.e., when the heterogeneity is not small. This was also observed for viscous fingering by Waggoner et al (1992), Sorbie et al (1994), and Li and Lake (1995) for miscible displacement and by Chang et al (1993) for immiscible displacement. At moderate heterogeneity channels form along the high permeability streaks and the development of CO_2 plumes strongly correlates with the permeability distribution of the field. The effect of large heterogeneity depends on the arrangement of the permeability field. Up to $1 < \lambda_R < 3$ there is no bypassing and the dissolution of CO_2 in water can be characterized by a dispersion model, which employs an effective dispersion coefficient to account for dissolution or transfer rate of CO_2 into water. When the correlation length is large the

estimated V_{DP} of the field becomes lower and therefore channeling regime occurs. At very large λ_R values the medium becomes layered and thus channels will form. This is summarized in Figure 13.

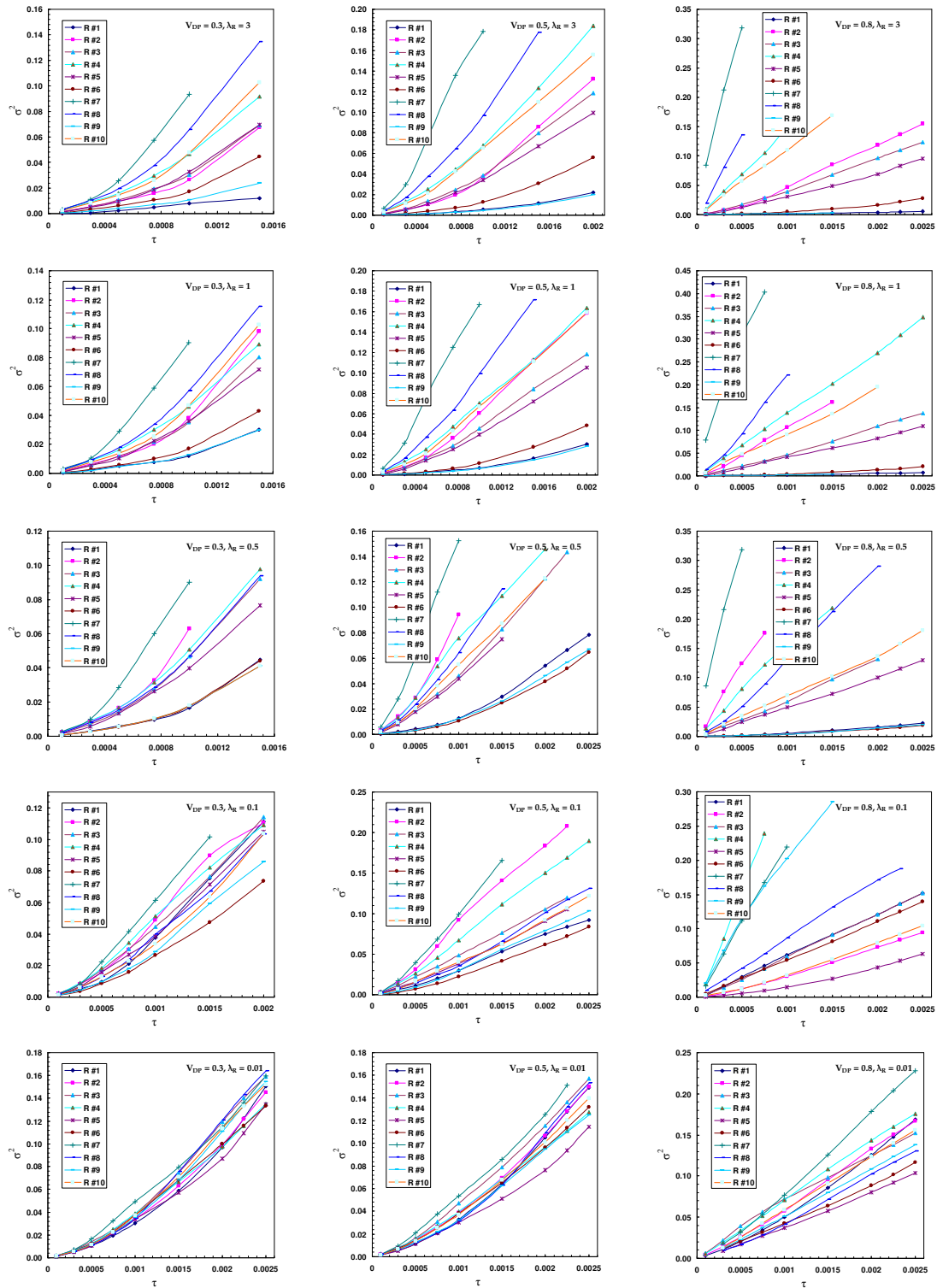


Figure 11: Variance of the average concentration in the medium a function of dimensionless time for multiple realizations of different simulations.

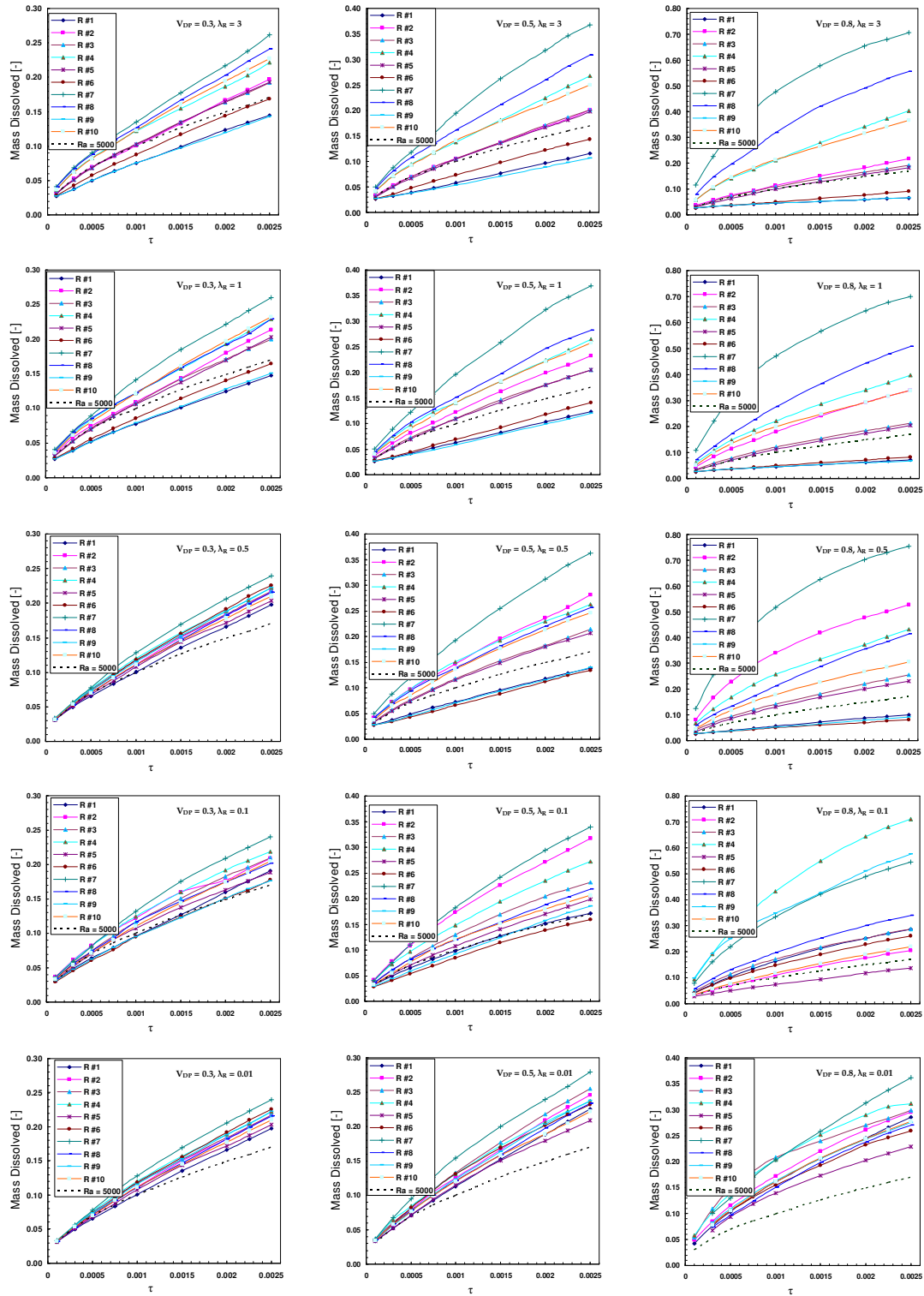


Figure 12: Dimensionless mass of dissolved CO₂ as a function of dimensionless time for multiple realizations of different simulations.

For our simulation conditions, efficient storage of CO₂ occurs in the heterogeneous reservoirs with small correlation length, although for all heterogeneous cases of practical relevance the transfer rates are higher than for the homogenous case. This suggests that simulations in the homogenous porous media are not realistic and underestimate the transfer rates. When studying the effect of heterogeneity on density-driven natural convection flow of CO₂ a single realization does not give a representative estimate of the transfer rate; therefore, more realizations are required to estimate the variance of the transfer rates between the realizations. Moreover, we find no correlation between the mass of dissolved CO₂ with the heterogeneity measures.

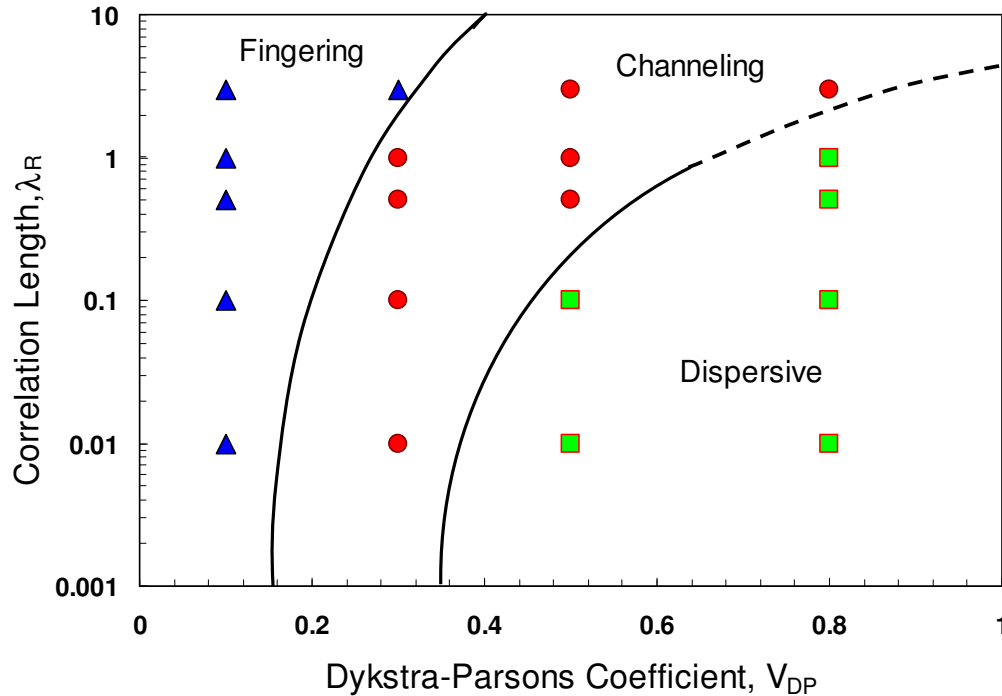


Figure 13: Flow regime map for density-driven natural convection ($Ra = 5000$).

5. Conclusions

- Following the work of Waggoner et al (1992) we studied the effect of heterogeneity on the character of natural convection flow when CO₂ overlays a brine column.
- Heterogeneity of the permeability (or Rayleigh) fields was characterized through a Dykstra-Parsons coefficient, V_{DP} , and their spatial arrangement was represented by a dimensionless correlation length, λ_R . We generated 10 realizations for each permeability field.
- Our numerical simulations demonstrate three flow regimes (fingering, dispersive, and channeling) for density-driven natural convection flow in heterogeneous media.
- At low heterogeneity characterized by small V_{DP} 's gravity-induced fingering is dominant pattern. Fingering will not occur in realistic porous media.
- At moderate heterogeneity (medium V_{DP} 's or large V_{DP} 's with large λ_R) the flow is dominated by the permeability field structure, i.e., channels form and CO₂ plumes progress along the high permeability streaks.
- At large heterogeneity when the correlation length of the field is small the flow is dispersive. In this regime the concentration travels proportional to square root of time and therefore it can be represented by a dispersion model.
- Numerical simulations in homogenous porous media underestimate the mass transfer rate of CO₂ into water. The rate of CO₂ dissolution in heterogeneous media is larger than in homogeneous media. This means that larger volumes of CO₂ can be stored in heterogeneous media.
- We found no correlation between the mass of dissolved CO₂ in water and the heterogeneity measures.

6. Nomenclature

A	Aspect ratio, H/L [-]
c	Dimensionless concentration [-]
c'	Concentration [mole/m^3]
D	Diffusion coefficient [m^2/s]
g	acceleration due to gravity [m/s^2]
H	Height of the porous medium [m]
k	Permeability of the porous medium [m^2]
L	Length of the porous medium [m]
p	Pressure [Pa]
Ra	Rayleigh number [-]
t	Time [sec]
u	Dimensionless velocity [-]
U	Velocity [m/s]
V_{DP}	Dykstra-Parsons coefficient
Z	Distance from the bottom of the tube [m]
X	Dimensionless distance in X coordinate
Z	Dimensionless distance in Z coordinate

Greek symbols

β_c	Volumetric expansion factor [m^3/mole]
δ	Amplitude [-]
φ	Porosity of the porous medium [-]
λ_R	Dimension less correlation length [-]
μ	Viscosity of the fluid [kg/m-sec]
ψ	Stream function [$\text{m}^3 \text{m}^{-1} \text{sec}^{-1}$]
ρ	Density of the fluid [kg/m ³]
σ	Standard deviation, square root of variance [-]
τ	Dimensionless time [-]

Subscripts

o	Value of the quantity at the boundary
i	Reference value of the quantity
x	Quantity in x -direction
z	Quantity in z -direction

7. References

- Bárdossy, A. *Copula-based geostatistical models for groundwater quality parameters*, Water Resources Research 42 (11) (2006) no. W11416.
- Borges, M.R., Pereira, F., Amaral Souto, H.P. *Efficient generation of multi-scale random fields: a hierarchical approach*. Communications in Numerical Methods in Engineering doi:10.1002/cnm.1134 (2009).
- Bruining, J., 1992, *Modeling reservoir heterogeneity with fractals: Enhanced Oil and Gas, Recovery Research Program*, Rep. No. 92-5, Center for Petroleum and Geosystems Engineering, Univ. of Texas, Austin, 88 p.
- Bruining, J.; Batenburg, D.W. van; L.W. Lake; Yang, A.P. *Flexible spectral methods for the generation of random fields with power-law semivariograms*. Mathematical Geology, 29, p. 823-848 (1997) . ISSN: 0882-8182.
- Chang, Y.B.; G. A. Pope; K. Sepehrnoori. *CO₂ Flow Patterns Under Multiphase Flow: Heterogeneous Field-Scale Conditions*. SPE Reservoir Engineering, 9(3) (1993) 208-216.
- Dake, L.P., *Fundamentals of Reservoir Engineering*, Developments in Petroleum Science 8, Elsevier, (1978)
- Dekking F.M., Kraaikamp, C., Elfeki, A.M., and Bruining, J. *Multiscale and multiresolution stochastic modelling of subsurface heterogeneity by tree-indexed Markov chains*. Computational Geosciences 5 (1) (2001) 47-60.
- Deutsch, C.V., and Journel, A.G., 1992, *GSLIB; Geostatistical Software Library and user's guide*: Oxford Univ. Press, New York, 340 p.
- Ennis-King, J. and Paterson, L.; *Role of convective mixing in the long-term storage of carbon dioxide in deep saline aquifers*, SPE J (2005) 10 (3), 349.
- Ebrahimi, F. and Sahimi, M. *Grid coarsening, simulation of transport processes in, and scale-up of heterogeneous media: Application of multiresolution wavelet transformations*, Mechanics of Materials 38 (2006) 772-785
- Elfeki, A.M.M., Dekking, F.M., Kraaikamp, C. & Bruining, J. *Influence of fine-scale heterogeneity patterns on large-scale behaviour of miscible transport in porous media*. Petroleum Geosciences", Vol 8 (2) (2002) 159-165.
- Farajzadeh, R.; Salimi, H.; Zitha, P.L.J.; Bruining, J. *Numerical Simulation of Density-Driven Natural Convection with Application for CO₂ Injection Projects*, Int. J. Heat and Mass Transfer (2007a), 50, 5054.
- Farajzadeh, R.; Barati, A.; Delil, H.A.; Bruining, J.; Zitha, P.L.J. *Mass Transfer of CO₂ into Water and Surfactant Solutions*, Petrol. Sci. and Technol., (2007b), 25, 1493.

- Farajzadeh, R.; Delil, H.A.; Zitha, P.L.J.; Bruining, J. *Enhanced Mass Transfer of CO₂ into Water and Oil by Natural Convection*, SPE 107380, EUROPEC London, The UK (2007c).
- Farajzadeh, R.; Farshbaf Zinati, F.; Zitha, P.L.J.; Bruining, J., *Density driven natural convection in layered and anisotropic porous media*, Proc. 11th European Conference on Mathematics in Oil Recovery (ECMOR X1), Bergen, Norway, 8-11 September (2008).
- Farajzadeh, R.; J. Bruining; Zitha, P.L.J. *Enhanced mass transfer of CO₂ into water: experiment and modeling*. Ind. Eng. Chem. Res. (2009) 48 (9), pp. 4542-4552.
- Gelhar, L. W. *Stochastic subsurface hydrology*. Prentice Hall Professional Technical Reference, 1993.
- Gelhar L.W. and C.L. Axness, *Three-dimensional stochastic analysis of macrodispersion in aquifers*, Water Resour. Res. 19 (1) (1983), pp. 161-180.
- Gmelin L., *Gmelin Handbuch der anorganischen Chemie*, 8. Auflage. Kohlenstoff, Teil C3, Verbindungen., pp 64-75 (1973).
- Green, C.; J. Ennis-King, K. Pruess. *Effect of Vertical Heterogeneity on Long-Term Migration of CO₂ in Saline Formation*. Energy Procedia (2009) 1(1) pp 1823-1830.
- Güçeri S. and Farouk B., *Numerical solutions in laminar and turbulent natural convection*, In: Natural convection, Fundamentals and applications, S. Kakac, W. Aung, R. Viskanta, Hemisphere publication, 615-655 (1985).
- Gunn R. D. and W. B. Krantz, *Reverse combustion instabilities in tar Sands and coal*, SPE 6735-PA (1980).
- Haugen, K.B. and A. Firoozabadi. *Composition at the interface between multi-component nonequilibrium fluid phases*. J. Chem. Phys. 130 (2009), 064707.
- Jensen, J.L., and Lake, L.W., 1988, The influence of sample size and permeability distribution on heterogeneity measures: SPE Reservoir Engineering v. 3, no. 2, p. 629-637.
- Jensen, J. L.; L. W. Lake; P. Corbett; D. Goggin. *Statistics For Petroleum Engineers And Geoscientists 2nd edition handbook of petroleum exploration and production 2 (HPEP)*. Elsevier, Dec. 2000.
- Journel, A.G. and Huijbregts, C.J., 1978, *Mining geostatistics*: Academic Press, London, 600 p.
- King, M.J., Blunt, M.J., Manseld, M., and Christie, M.A., 1993, *Rapid evaluation of the impact of heterogeneity on miscible gas injection*: Proc. 7th European Symp. on IOR, (Moscow, Russia), v. 2, p. 398-407.
- Koval, E. J. *A Method for Predicting the Performance of Unstable Miscible Displacement in Heterogeneous Media*. SPE J. 3(2) (1963) 145-154.
- Landau, L.D. and E.M. Lifshitz, *Statistical Physics: Course of Theoretical Physics Volume 5*, 2nd revised English Ed., Pergamon Press (1969).
- Lasseter, T.J., Waggoner, J.R., and Lake, L.W., 1986, Reservoir heterogeneity and its influence on ultimate recovery, Lake, L.W. and Carroll, H.B., eds., *Reservoir characterization*: Academic Press, Orlando, Florida, 659 p.
- Li, D. and L. W. Lake, *Scaling Fluid Flow Through Heterogeneous Permeable Media*, SPE Advanced Technology, 3(1), (1995) 188-197.
- Meulenbroek, B.; R. Farajzadeh; J. Bruining, *Multiple scale analysis of the stability of a diffusive interface between aqueous and gaseous CO₂*, Submitted to J. Fluid Mechanics, 2010.
- Nathan D. Monnig, David A. Benson, and Mark M. Meerschaert, Ensemble solute transport in two-dimensional operator-scaling random fields, *Water Resources Research*, Vol. 44, W02434, doi:10.1029/2007WR005998, 2008
- Nield, D.A. and C.T. Simmons. *A discussion on the effect of heterogeneity on the onset of convection in a porous medium*. *Transp. Porous Media* 68 (2007) 413-421.
- Park C.W., Gorell S and Homsy G.M., *Two-phase displacement in Hele-Shaw cells: experiments on viscosity driven instabilities*, *J. Fluid Mech.*, 141, 275-287 (1984).
- Parlar, M. and Y. C. Yortsos, *Percolation theory of steam/water relative permeability*, SPE 16969 (1987).
- Press, W.H., Teukolsky, S.A., Vetterling, W.T., and Flannery, B.P., *Numerical Recipes in C, The Art of Scientific Computing*, 2nd edition, Cambridge University Press (1992).
- Ranganathan, P.; J. Bruining, P.L.J. Zitha. *Numerical Simulation of Natural Convection in Heterogeneous Porous media for CO₂ Geological Storage*. To be published in *Transport in Porous Media* (2010).
- Riaz A., Hesse M., Tchelepi A. and Orr F.M., *Onset of convection in a gravitationally unstable diffusive boundary layer in porous medium*, *J. Fluid Mech.*, 548, 87-111 (2006).
- Rice, S.O. *Mathematical analysis of random noise*, Wax, N.ed., Selected papers on noise and stochastic processes: Dover Publ., New York, p.133-294.
- Shinozuka, M., and Jan, C.M., 1972, *Digital simulation of random processes and its applications*: Jour. Sound and Vibration, v. 25, no. 1, p. 357-368.
- Sahimi, M., 2005. *Flow and Transport in Porous Media and Fractured Rock*, second ed. VCH, Weinheim, Germany
- Sorbie, K. S.; Farag Feghi; K. S. Pickup; P. S. Ringrose, and J. L. Jensen. *Flow Regimes in Miscible Displacements in Heterogeneous Correlated Random Fields*. SPE Advanced Technology Series, 2(2) (1994) pp 78-87.
- Vanmarcke, E. *Random field analysis and synthesis*: 1983, M.I.T.Press, Cambridge, Massachusetts, 382p.
- Waggoner, J.R., Castillo, J.L., and Lake, L.W. *Simulation of EOR processes in stochastically generated permeable media*, SPE Formation Evaluation (1992) v. 7, no. 2, p. 173-180.
- Weir, G. J.; White S.P.; W.M. Kissling. *Reservoir Storage and Containment of Greenhouse Gases*, Energy Convers. Mgmt., (1995), 36, No. 6-9, 531.
- Xu X., Chen Sh. And Zhang D., *Convective stability analysis of the long-term storage of carbon dioxide in deep saline aquifers*, Adv. Water Res., 29, 397-407 (2006).

Yang, A.P., and Lake, L.W. *The Accuracy of autocorrelation estimates*. In Situ (1989) 12(4) 227-274.

Yang Ch. and Gu Y., *Accelerated mass transfer of CO₂ in reservoir brine due to density-driven natural convection at high pressures and elevated temperatures*, Ind. Eng. Chem. Res., 45, 2430-2436 (2006).

Yortsos, Y. C., B. Xu and D. Salin, *Phase Diagram of Fully Developed Drainage in Porous Media*, Physical Review Letters, Vol 79, No. 23 (1997).